*Mária Macáková, Jan Beňa**)

Simple Changes of an Object Studied by Hologram Interferometry

Part II

The rotations of a diffusely reflecting object are investigated by double exposure hologram interferometry. A detailed analysis of the fringe formation and localization conditions are given for a general observation point. The theoretical predictions are verified in the case of rotation about an axis lying in the object surface and normal to it.

1. Introduction

An application of holographic interferometry is in the investigation of the general changes of an object. In classical interferometry one reflecting surface is compared with another one. On the other hand in holographic interferometry an object is compared with the same one after it has been changed. As was shown by STETSON [3], [4], even small vibrations of an object can be investigated in this same manner. The theoretical treatment is more complicated, because the interference fringes are localized in a relatively small region of space. However, the information about the fringe localization can help us to interprete the change in the object from the fringe pattern. The first attempts [1], [2] to find the localization conditions suffered from certain limitations. The general solution of this problem has been achieved by STETSON [3], [4].

In this paper we are concerned with object rotations, investigated by double exposure holographic interferometry. Our futher considerations are based on Stetson's formulation of the problem. The alternative derivation of the formulae for fringe geometry is given.

2. Object Rotations

Let us consider the amplitude $w(\boldsymbol{r}, t)$ of the object wave field at any point $\boldsymbol{r}$ in space. The time dependence of this amplitude arises from various changes (translations, rotations, deformations) of the object. After reconstruction of the hologram the wave field has an amplitude $b(\boldsymbol{r})$ at the point $\boldsymbol{r}$ which represents the time average of $w(\boldsymbol{r}, t)$ (denoted as $\langle\ \rangle$) during the hologram exposure. This amplitude can be related to the Fourier spectrum of the object through the Rayleigh integral formula [3]

$$b(\boldsymbol{r}) = \langle w(\boldsymbol{r}, t)\rangle = \\ = \int\int \varphi(k_{2x}, k_{2y})\, M(\Phi)\, A(\boldsymbol{k}_2, \boldsymbol{r})\, e^{i\boldsymbol{k}_2\cdot\boldsymbol{r}}\, dk_{2x} dk_{2y}. \quad (1)$$

Here $\varphi(k_{2x}, k_{2y})$ is the amplitude of the Fourier plane wave component of the object field. The reference system x, y, z is related to the object surface $(x, y)\cdot$ $\cdot\Phi(\boldsymbol{k}_2, \boldsymbol{r})$ is a phase factor arising from the object changes. $M(\Phi) = \langle e^{i\Phi}\rangle$ represents the characteristic fringe function which is given by,

$$M(\Phi) = \cos\frac{\Phi}{2} \quad \text{if the motion is two valued}$$

$$M(\Phi) = I_0\left(\frac{\Phi}{2}\right) \quad \text{if the motion is sinusoidal.}$$

In general Φ depends upon the illumination vector $\boldsymbol{k}_1$, the direction of the scattered light $\boldsymbol{k}_2$ and on the point of observation $\boldsymbol{r}$. A very important case arises when Φ is nearly independent of $\boldsymbol{k}_2$ in some region of the space. Then the characteristic function $M(\Phi)$ may be taken outside the integral sign. Now it is clear that the object time averaged wave field is essentially modulated by the function $M(\Phi)$. This modulation implies localized interference fringes in such a region. Thus all the information about the geometry and visibility of the hologram interference fringes is contained in characteristc fringe function $M(\Phi)$. Since usually the interference pattern is observed through an optical system, its influence on the fringe visibility is involved through the aperture function $A(\boldsymbol{k}_2, \boldsymbol{r})$.

*) Faculty of Engineering, Slovak Technical University Bratislava, Gottwaldovo nám. 50, Czechoslovakia.

Now the condition for the fringe localization may be expressed as

$$\nabla_{k_2} M(\Phi) \cong 0. \tag{2}$$

The fringe geometry is specifed from

$$M(\Phi) = \text{const}. \tag{3}$$

Let us consider an idealized optical system with a small aperture Δ. The optical axis of this system is parallel to the k_{20} which means that,

$$A(k_2) = 1, \quad \text{if} \quad |k_2 - k_{20}| < \Delta \quad (\Delta << k_2)$$

otherwise $A(k_2) = 0$. Expanding $M(\Phi)$ in a Taylor series about k_{20} we obtain

$$b(r) = M(\Phi_0) \iint\limits_{|k_2 - k_{20}| < \Delta} \varphi A e^{ik_2 \cdot r} dk_2^2 + \\ + \frac{\partial M}{\partial k_{2x}} \iint\limits_{|k_2 - k_{20}| < \Delta} \varphi A e^{ik_2 \cdot r} \Delta k_{2x} dk_2^2 + \\ + \frac{\partial M}{\partial k_{2y}} \iint\limits_{|k_2 - k_{20}| < \Delta} \varphi A e^{ik_2 \cdot r} \Delta k_{2y} dk_2^2. \tag{4}$$

The first integral is the stationary object field multipled by the fringe function $M(\Phi_0)$. As has been shown by STETSON [4] the second two terms for the diffuse object behave as a noise function. From this it follows that the maximum fringe visibility occurs when the two noise terms in eq. (4) are negligible.

Now we are concerned with simple rotations without mutual translation of the object (this means that the rotation axis intersects the object surface or lies on the surface). Let us consider that the object is illuminated by a plane wave

$$A e^{ik_1 \cdot r}. \tag{5}$$

If we are dealing with the diffuse reflecting object we must take into account that this surface is rough. Then the wave $A e^{ik_1 \cdot r}$ is modulated by the surface transfer function $p(r)$. By expanding $p(r)$ into a Fourier series we obtain

$$p(r) = \sum_G P(G) e^{iG \cdot r}. \tag{6}$$

Here $P(G)$ represents a spectral amplitude of the surface for a general space frequency expressed by G. Multiplying the function (5) by the surface transfer function (6) an expressions for the wave field scattered by the object is obtained

$$b = \sum_G A P(G) e^{i(k_1 + G) \cdot r}, \tag{7}$$

where $\tilde{k}_1 = k_{1x} i + k_{1y} j$. This field may be regarded, according to the Rayleigh integral formula [3], as a superposition of the plane waves propagating with a vector k_2 defined as follows

$$|k_2| = |k_1|, \quad k_2 = k_1 + G, \tag{8}$$

where $\tilde{k}_2 = k_{2x} i + k_{2y} j$. Now, each scattered plane wave component may be regarded as a wave diffracted on the sinusoidal grating lateral to G with period $a = \frac{2\pi}{|G|}$. If the object undergoes any changes, the relation (8) must still be satisfied.

First we introduce the unit normal n to the surface. Usually k_1 and k_2 are known so an expression for G must be found. The absolute value $|\tilde{k}_2 - \tilde{k}_1|$ may be obtained from the vector product $(k_2 - k_1) \times n$. However $(k_2 - k_1) \times n$ is perpendicular to the $\tilde{k}_2 - \tilde{k}_1$. Multiplying by n once we get

$$G = n \times [(k_2 - k_1) \times n]. \tag{9}$$

As the object changes so all the vectors of interest are changed accordingly,

$$G \to G'$$
$$n \to n'$$
$$k_2 \to k_2'.$$

Substituting into eq. (9) we have

$$G + \Delta G = (n + \Delta n) \times [(k_2 + \Delta k_2 - k_1) \times (n + \Delta n)]. \tag{10}$$

Neglecting the terms of the higher order Δk_2, Δn eg. (10) gives

$$\Delta G = n \times [(k_2 - k_1) \times \Delta n] + \Delta n \times [(k_2 - k_1) \times n] + \\ + n \times (\Delta k_2 \times n). \tag{11}$$

After rearrangement we find that,

$$\Delta k_2 = \Delta G + n \Delta k_{2n} + (k_2 - k_1)(\Delta n\, n + n \Delta n). \tag{12}$$

This is the basic equation for calculating the changes Δk_2. It determines two components Δk_2. The third component is with regard to eq. (8)

$$\Delta k_2 \cdot k_2 = 0. \tag{13}$$

Since our coordinate system is chosen so that the z-axis is parallel to the n and the x, y axes lie in the surface plane, eqs. (12), (13) may be written as

$$\Delta k_{2x} = \Delta G_x + (k_{2z} - k_{1z}) \Delta n_x, \\ \Delta k_{2y} = \Delta G_y + (k_{2z} - k_{1z}) \Delta n_y, \tag{14} \\ \Delta k_{2z} = -\frac{k_{2x}}{k_{2z}} \Delta k_{2x} - \frac{k_{2y}}{k_{2z}} \Delta k_{2y}.$$

Note:
Our definition of the grating vector G differs from that of Stetson in that we multiply by n twice. This

is advantageous because there is no need to distinguish the change $\Delta \boldsymbol{k}_2$ of the illumination from the change $\Delta \boldsymbol{k}_2$ of observation.

x-axis rotation

x-axis rotation in this paper will mean any rotation of the object about an axis lying on the object surface (see Fig. 1). The coordinate system x, y, z is

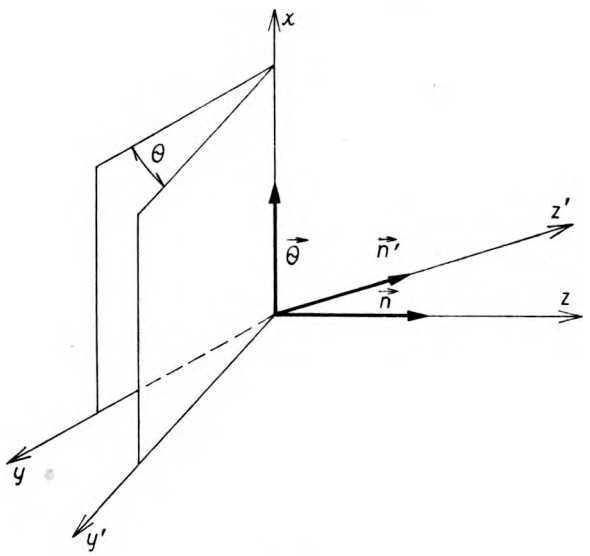

Fig. 1

located on the object surface. The rotation is characterized by the vector $\boldsymbol{\Theta} = \Theta \boldsymbol{i}$. Then it can be written that

$$\Delta \boldsymbol{G} = \boldsymbol{\Theta} \times \boldsymbol{G}, \quad (\boldsymbol{G} = G_x \boldsymbol{i} + G_y \boldsymbol{j}), \qquad \Delta \boldsymbol{n} = \boldsymbol{\Theta} \times \boldsymbol{n}. \tag{15}$$

Rewriting eq. (14) for this case we get

$$\Phi = \Delta \boldsymbol{k}_2 \cdot \boldsymbol{r} = y(k_{1z} - k_{2z})\Theta - z \frac{k_{2y}}{k_{2z}} (k_{1z} - k_{2z})\Theta. \tag{16}$$

From the localization conditions $\dfrac{\partial \Phi}{\partial k_{2x}} = \dfrac{\partial \Phi}{\partial k_{2y}} = 0$ it follows $y = z = 0$, i. e. interference fringes are localized along the *x*-axis. $\left(\text{In finding } \dfrac{\partial k_{2z}}{\partial k_{2x}} \text{ we have utilized the fact } k_{2x}^2 + k_{2y}^2 + k_{2z}^2 = \left(\frac{2\pi}{\lambda}\right)^2\right)$.

When observing the fringes in the $\boldsymbol{n}_{20}$ direction the fringe form is given by equation

$$y(n_{1z} - n_{20z})\Theta - z \frac{n_{20y}}{n_{20z}} (n_{1z} - n_{20z})\Theta = m\lambda, \tag{17}$$

where m is an integer. Let us introduce a new reference frame ξ, η, ζ. Let the ζ-axis be parallel to the $\boldsymbol{n}_{20}$ direction. Further analysis becomes very simple if we choose the ζ-axis parallel to the rotation axis x. The origin of the new reference frame is the same as that of the old one. Now for the fringes in the $\zeta = 0$ plane one has

$$\eta_m = \frac{m\lambda n_{20z}}{(n_{1z} - n_{20z})\Theta}. \tag{18}$$

This means that fringes are straight lines parallel to the ξ-axis and to the rotation axis too. The fringe spacing is

$$d = \frac{\lambda n_{20z}}{(n_{1z} - n_{20z})\Theta}. \tag{19}$$

This result is well known in classical interferometry as interference between two planes with a small angle between them.

z-axis rotations

Let us now consider rotations about *z*-axis which is normal to the object surface. There is no analogy in classical interferometry for this case. The rotation is specified by the vector $\boldsymbol{\Theta} = \Theta \boldsymbol{k}$. Substitution of corresponding variables into eq. (14) gives

$$\Phi = \left\{ \left[k_{2y} \left(-x + z \frac{k_{1x}}{k_{2z}} \right) - k_{2x} \left(-y + z \frac{k_{1y}}{k_{2z}} \right) \right] + x k_{1y} - y k_{1x} \right\} \Theta \tag{20}$$

If $\boldsymbol{k}_1, \boldsymbol{k}_2$ and $\boldsymbol{n}$ are in the same plane, the localization conditions are simplified to the form:

$$\left.\begin{aligned} y &= z \frac{k_{1y}}{k_{2z}} \\ x &= z \frac{k_{1x}}{k_{2z}} \end{aligned}\right\} \Rightarrow \frac{y}{x} = \frac{k_{1y}}{k_{1x}}. \tag{21}$$

Eqs. (21) implies that fringes are localized along a straight line. It holds true that for its direction $\boldsymbol{v}$

$$\left.\begin{aligned} v_x &= \frac{k_{1x}}{\sqrt{k_{1x}^2 + k_{1y}^2 + k_{2z}^2}}, \\ v_y &= \frac{k_{1y}}{\sqrt{k_{1x}^2 + k_{1y}^2 + k_{2z}^2}}, \\ v_z &= \frac{k_{2z}}{\sqrt{k_{1x}^2 + k_{1y}^2 + k_{2z}^2}}. \end{aligned}\right\} \tag{22}$$

The geometry of the fringes is determined by eq. (20) Without loss of generality the *x*-axis may be

located perpendicular to the $\boldsymbol{k}_1$ and $\boldsymbol{k}_2$ vectors. Then we introduce a new coordinate system ξ, η, ζ as in the previous case. (There $\zeta \| \boldsymbol{n}_{20}$, $\xi \| x$, $\eta_0 = \zeta_0 \times \xi_0$.) Now, substitution of the new variables into eq. (20) gives, remembering that $n_{1x} = n_{2x} = 0$ for this case

$$m\lambda = \xi(n_{1y} - n_{2y})\Theta. \tag{23}$$

For the fringe spacing near the object surface ($\zeta = 0$) it follows that

$$d = \frac{\lambda}{(n_{1y} - n_{20y})\Theta}. \tag{24}$$

It can be seen from eqs. (23) and (24) that the interference fringes are parallel to the plane containing $\boldsymbol{k}_1, \boldsymbol{k}_{20}, \boldsymbol{n}$ in this case.

3. Experimental Results

A diagram of the experimental set up is shown in Fig. 2. A beam from a 5 mW He–Ne laser passes through a shutter Z and beam splitter M_1. The reference and object beams are expanded by microscopic

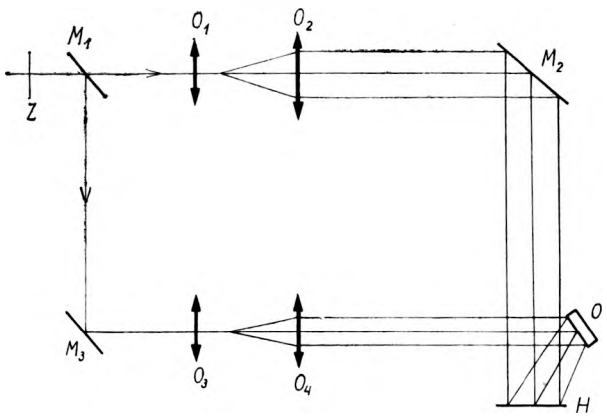

Fig. 2. Diagram of the experimental set up. Abbreviations: Z – shutter, M_1 – beam splitter, M_2, M_3 – mirrors, O_1, O_3 – microscope lenses, O_2, O_4 – lenses, O – object, H – hologram

lenses O_1, O_3 and collimated by lenses O_2, O_4. The reference beam is directed by the mirror M_2 onto the hologram The object O (an aluminium plate $14 \times 21 \times 31$ mm^3) is placed on a precision goniometer (Präzisions Mechanik SGO 101) for x-axis rotations. With the appartus, it is possible to determine the angle Θ within 2″ accuracy. The illumination of the processed hologram by the object beam gives the reconstructed wavefront with a high intensity.

The calculations were based on eq. (19). The observation angle ϑ_2 we have chosen is the same as the incident angle ϑ_1. Setting $n_{20z} = -n_{1z}$ into eq. (19) we obtain

$$d = \frac{\lambda}{2\Theta}, \tag{25}$$

where d is the fringe spacing in the plane $\zeta = 0$, involving the axis of rotation ξ. Figure 3 shows an

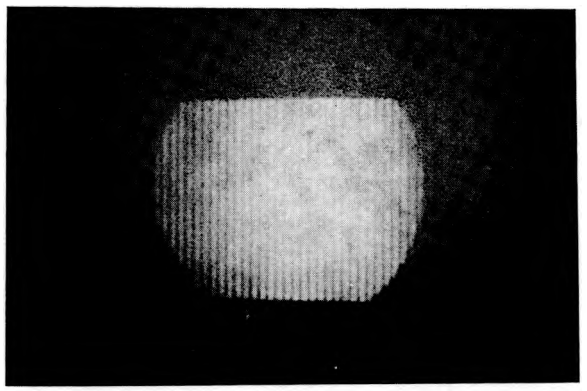

Fig. 3. Example of the interference pattern for the object rotation $\Theta = 78''$ about x-axis

interference pattern for the object rotation $\Theta = 78''$. The calculated and actual values are compared in Tab. 1. This case is well known in classical interferometry and therefore we shall not deal with it further.

Table 1

Θ meas.	Θ calc.	Error
20″	22″	2″
40″	38.5″	−1.5″
60″	70″	10″
78″	75″	−3″
102″	105″	3″
122″	125″	3″

In plane rotations (z-axis rotations) have been realized with help of the precise dividing head Somet M3-485. This enabled the angle Θ to be read within 1′ accuracy. The angle of incidence was $\vartheta_1 = 31°$ and the angle of observation was $\vartheta_2 = 40°20'$. The components of the unit vectors $\boldsymbol{n}_1, \boldsymbol{n}_{20}$ were,

$$\begin{aligned} n_{1x} &= 0 \quad n_{1y} = -0.515 \quad n_{1z} = -0.857 \\ n_{2x} &= 0 \quad n_{2y} = -0.647 \quad n_{2z} = 0.762. \end{aligned} \tag{26}$$

Under these circumstances we get for the rotation angle

$$\Theta = \frac{\lambda}{(n_{1y} - n_{2y})d} = \frac{\lambda}{0.132d}, \tag{27}$$

where d is the fringe spacing in the plane $\zeta = 0$. This plane is perpendicular to the line of sight and passes through the point where the rotation axis intersects the object surface.

In plane rotations do not have any analogy in classical interferometry. The fringe localization along a line in space was obvious in this case as is demonstrated in Fig. 4a, b, c.

The center of the resolved fringes was approximately at the object boundary in the cases a, and c, in Fig. 4. We have attempted to specify the line of localization from this fact. The components of r are

$$r_x = 0, \quad r_y = -0.58, \quad r_z = 0.81.$$

angle of observation ϑ_2 approaches the incident angle ϑ_1 the difference $n_{1y} - n_{20y}$ becomes smaller and the fringe spacing increases rapidly. The fringes are no longer parallel to each other, but they become hyperbolic. This can just be seen in Fig. 5c, but the effect is more obvious by visual observation of the interference fringe pattern. Therefore we have attempted to show this interesting fringe shape in Fig. 7. The four interference patterns were recorded from directions near to the critical angle $\vartheta_2 = \vartheta_1$. We had to

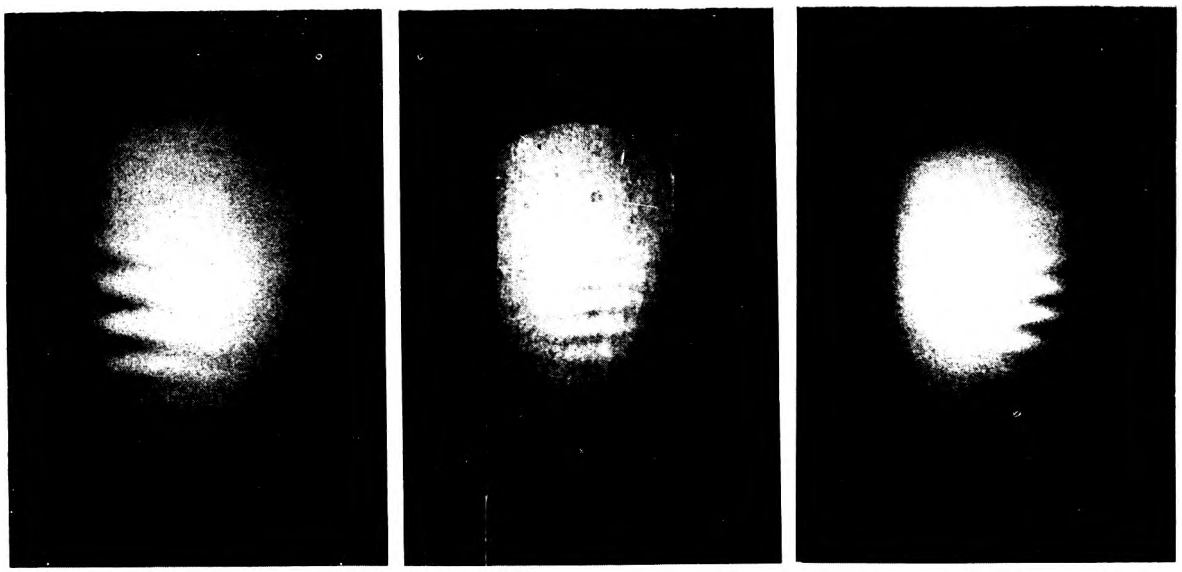

a b c

Fig. 4. The interference fringes produced from a double exposure hologram for z-axis rotation $\Theta = 8'$. Optical observing system with aperture 1:4.5 is focused at a — 84 mm in front of the object, b — at the object surface, c — at 102 mm behind the object

The equations (22) imply

$$r_x = 0, \quad r_y = -0.56, \quad r_z = 0.83.$$

There is good agreement between the experimental and theoretical values for the region where the interference fringes are localized. The fringe visibility and size of the localization area depend considerably on the aperture of the observing optical system. It is illustrated in Fig. 5a, b, c.

The densitometric curves for these interference patterns are shown in Fig. 6a, b. It can be seen clearly from this figure that the fringe contrast is better and the resolved fringe area is greater when the aperture is smaller.

From eq. (24) it follows, that as the value of the use very small apertures (1:22) to obtain well resolved interference fringes.

4. Summary

The x-axis rotations are the same as in classical interferometry. Therefore we have dealt with them briefly. Measurements of this kind were also carried out by FROEHLY *et al.* [5].

In plane rotations have not been mentioned yet, with the exception of STETSON'S papers [3], [4], [6]. Stetson has investigated the object vibrations. Because the vibration amplitude could not be controlled precisely, he did not compare his experimental and calculated values. In the case of z-axis rotations the basic features of holographic interferometry become very obvious. The fringes arise from the total object change

a

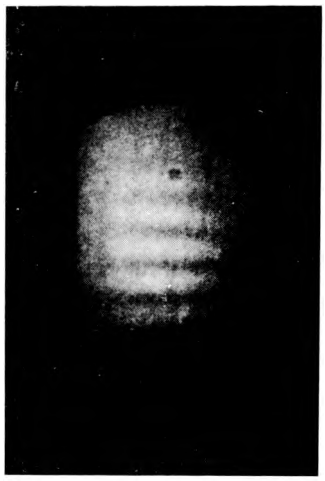

b

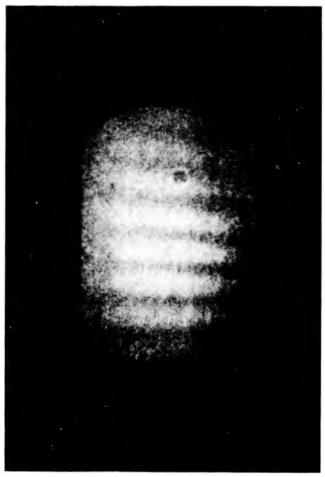

c

Fig. 5. The interference patterns for z-axis rotation $\Theta = 6'$ observed with a various circular aperture of the optical system a — aperture 1:4.5 b — aperture 1:5.6, c — aperture 1:8

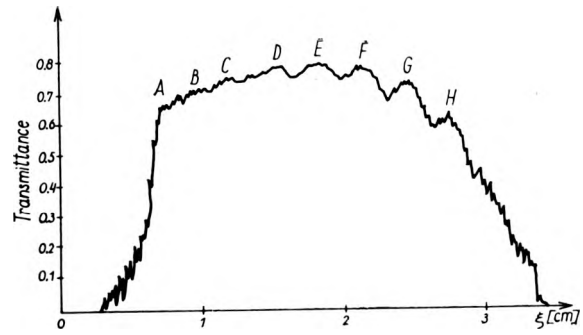

a

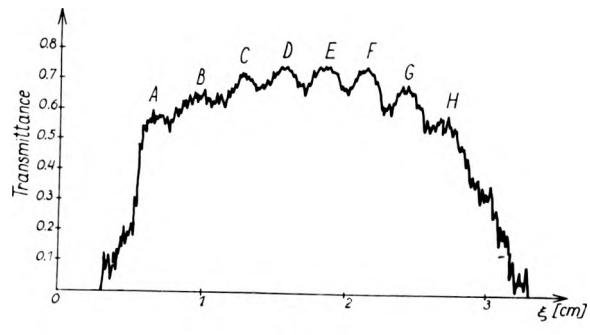

b

Fig. 6. The densitometric curves of the interference patterns produced from a double exposure hologram in the case z-axis rotation $\Theta = 6'$. The aperture of camera was a — 1:4.5, b — 1:8 respectively. A, B, C, D, E, F, G, H denote the interference maximum

and their visibility depends considerably on the observation point. The size and shape of the fringes depend on the direction of observation also. For the calculations it is necessary to know the directions of illumination and observation exactly and to know the magnifying factor of the optical system too. Only if these conditions are satisfied, accurate measurements can be made. The range of rotation angles which are

Table 2

Θ meas.	Θ calc.
2′	1′38″
4′	3′59″
6′	6′30″
8′	7′40″
10′	9′39″
12′	11′41″

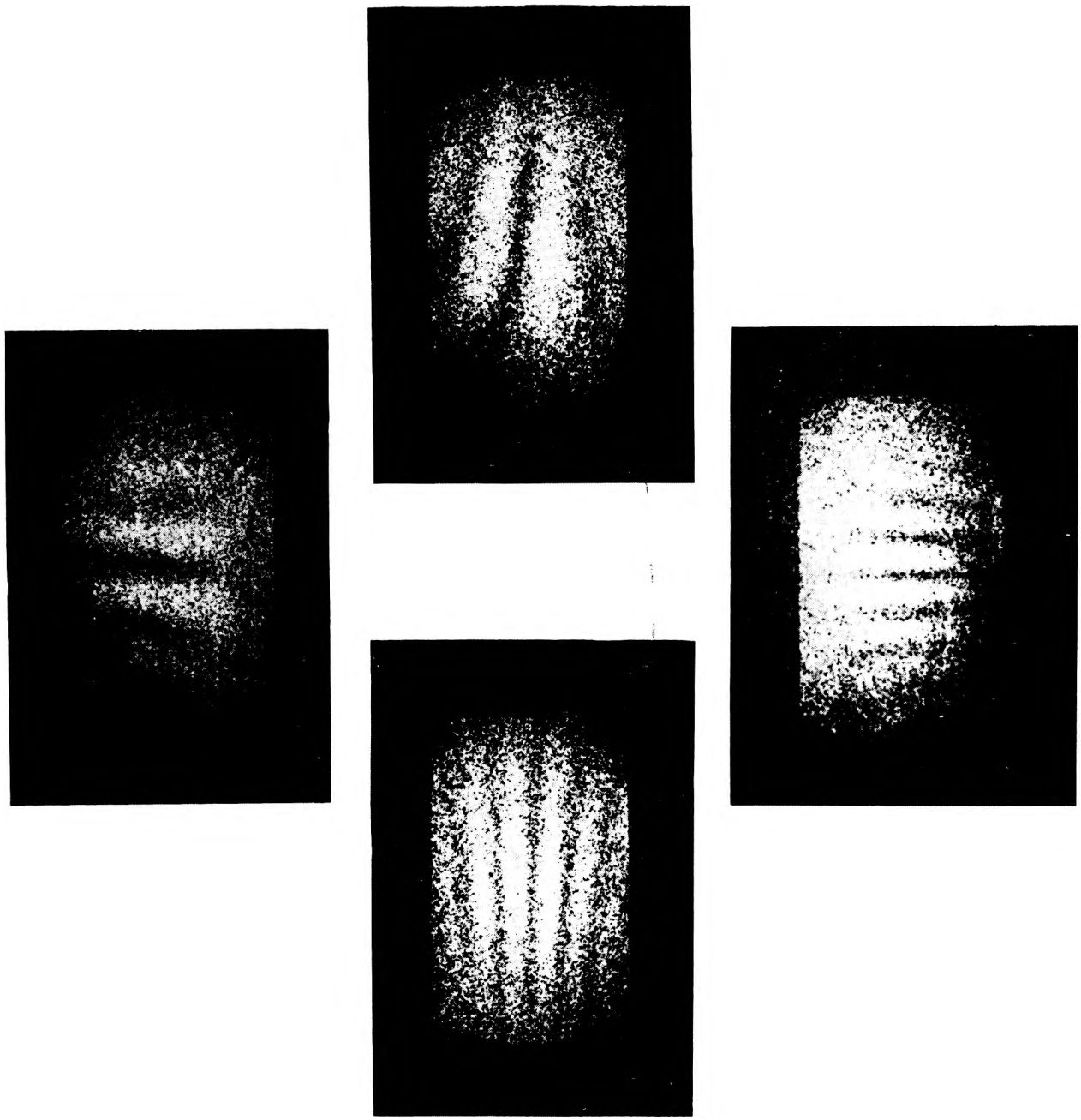

Fig. 7. Example of the interference patterns for the object rotation $\Theta = 30'$ about z-axis in the various directions near the critical angle $\vartheta_1 = \vartheta_2$. The pictures are arranged according to the directions of observation

measurable may be changed simply by a convenient choise of the observation angle. We have measured rotations in the range 2′–12′. There is good agreement between the calculated and actual values (Tab. 2). The observed fringe localization has confirmed the theoretical predictions.

Les changements simples de l'objet examiné par la méthode d'interférométrie holographique

A l'aide de la méthode d'interférométrie holographique on a examiné les rotations de l'objet réfléchissant par diffusion. On a présenté en détail l'analyse de la formation des franges et les conditions de la localisation des franges pour un point d'observation général. Les considérations théoriques sont vérifiées dans le cas où la rotation se fait autour de l'axe dans le plan-objet et aussi dans le cas de l'axe perpendiculaire au plan-objet.

Простые изменения объекта, исследуемого методом голографической интерферометрии

Вращения отражающего диффузионно объекта исследовались методом голографической интерферометрии. Дается подробный анализ формирования и условий локализации полос для общей точки наблюдения. Теоретические предположения проверены в случае вращения вокруг оси, расположенной в плоскости объекта, а также оси, препендикулярной к ней.

References

[1] Alexandrov E. B., Bonch-Bruevich A. M., Zhurn. Tekhn. Fiz. **37** (1967), 360.

[2] Tsuruta T., Shiotake N., Itoh J., Optica Acta **16** (1969), 723.

[3] Stetson K. A., *Symposium on the Engineering Uses of Holography*, Glasgow, Sept. 1968, Cambridge Press, Cambridge 1970.

[4] Stetson K. A., Optik **29** (1969), 386.

[5] Froehly C., Monneret J., Pasteur J., Vienot J. Ch., Optica Acta **16** (1969), 343.

[6] Molin N. E., Stetson K. A., Optik **31** (1970), 281.

Received, April 17, 1973